DOI 10.5162/sensor2017/B5.2

Computational Methods in Coherent Optical Metrology

Claas Falldorf[1], Mostafa Agour[1,2], Ralf B. Bergmann[1,3]
[1] BAS-Bremer Institut für angewandte Strahltechnik, Klagenfurter Str.5, 28359 Bremen, Germany,
[2] Faculty of Science, Department of Physics, Aswan University, Aswan 81528, Egypt,
[3] University of Bremen, MAPEX and Faculty 01: Physics and Electrical Engineering, 28359 Bremen
falldorf@bias.de

Abstract

We demonstrate that incorporating computational methods into the measurement process enables combining beneficial properties, such as short acquisition time, insensitivity to mechanical disturbances and high accuracy. We give the two examples of digital holography, which combines fast acquisition times with high precision, and computational shear interferometry which is precise and insensitive to mechanical vibrations at the same time.

Key words: Optical Inspection, Interferometry, Shear Interferometry, Digital holography, Computational methods

Introduction

The industrial trend towards increasing production efficiency, product complexity and faster production cycles demands novel types of measurement systems that combine intuitively contradicting properties, such as fast measurement speed, high flexibility, high accuracy and insensitivity to mechanical disturbances. In this publication we show that these requirements can be met by incorporating computational methods into the measurement process in coherent optical metrology. In contrast to standard image processing, the computational method represents an integral part of the measurement procedure in the sense, that we don't yield an interpretable result without it.

This relaxes the requirements for the physical setup and adds some degree of freedom with respect to the signal generation, because the recorded intensities do not need to be meaningful to a human observer. The added flexibility in the system design gives rise to new methods, which either combine the above mentioned beneficial properties or reduce system costs by mitigating demanding optical specifications, for example.

In analogy to similar efforts in the field of computational imaging, we therefore may refer to these techniques as computational optical metrology (CoMet). In the following we will discuss two examples that fall into this category, namely digital holography (DH) and computational shear interferometry (CoSI) in order to point towards the great benefits obtained from those techniques.

Examples

Digital Holography

Digital holography is based upon processing of a digital hologram $H(x)$, which is a recording of an interference pattern formed by superposition of light scattered by an object $U(x)$ and a coherent reference wave R(x) with known characteristics:

$$H=|U+R|^2=|U|^2+|R|^2+U^*R+R^*U. \quad (1)$$

In most cases the hologram is not directly interpretable by a human operator. If R is a plane wave which is tilted with respect to the optical axis (off-axis holography), the 4 terms in Eq.(1) separate in the frequency domain. In this case we can determine $U(x)$ by means a window filter $W(k_x,k_y)$ in the Fourier domain [1]:

$$U(x)=F^{-1}\{F\{H\cdot R\}\cdot W(k_x,k_y)\}. \quad (2)$$

In Eq.(2), F{...} denotes the Fourier transformation. Once $U(x)$ is determined, we can calculate propagated representations $U_z(x)$ of it by a numerical simulation of the free space propagation process, e.g.

$$U_z(x)=F^{-1}\{\widehat{U}(k_x,k_y)\exp[\mathrm{i}k_z z]\}. \quad (3)$$

In Eq.(3), $\widehat{U}$ is the Fouriertransform of $U(x)$, z is the propagation distance, and k_x, k_y and k_z are the components of the wave vector.

The propagation can be used for example to obtain digital images of the object in different object planes.

The numerical processing is inherently required to obtain the measurement result, making digital holography a computational method in the above sense. Having said this, digital holography provides some remarkable features, such as volumetric imaging capabilities [2] and the ability to perform 3D shape measurements [3] as well as quantitative phase contrast imaging [4] by evaluating the lateral phase distribution of $U_z(x)$ across the object plane. All of this can be obtained from recording of a single digital hologram, which can be captured within a fraction of a second, down to the nanosecond regime. A basic scheme of a digital holographic setup is shown in Fig.1, where the microscope objective (lens) is used to provide lateral resolution in the micrometer range.

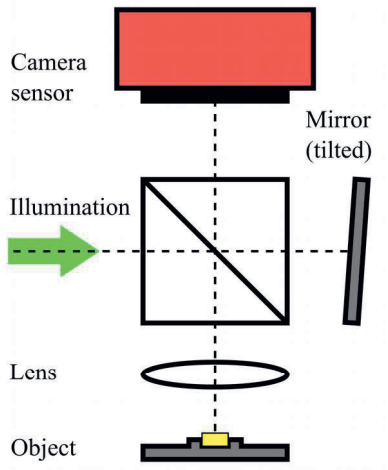

Fig.1.Scheme of a digital holographic setup with a microscope lens for high lateral resolution in the micrometer range. The light is incident from the left, indicated by the arrow. The mirror is slightly tilted to allow for off-axis holography.

However, it is not necessary that the camera sensor is located exactly in the image plane of the objective because of the refocusing capabilities of digital holography.

A plane wave is inserted from the left side as indicated by the arrow, where a beam splitting cube splits it into an object beam and a reference wave. The object beam illuminates the object and is reflected back towards the camera chip. The camera is operated without any lens objective. The reference wave is reflected from the mirror which is slightly tilted in order to allow for off-axis holography.

An example of a measurement is shown in Fig.2, where the 3D shape of the functional component of a micro-electro-mechanical switch is measured using digital holography [5]. Here, we used the relation

$$\varphi(x)=\frac{2\pi}{\lambda}2h(x) \qquad (4)$$

between the profile $h(x)$ of the object and the lateral phase distribution $\varphi(x)$ of $U_z(x)$ under normally incident object illumination.

Because of the combination between a short measurement time and high precision, digital holography has recently been qualified for in-line inspection in the production process of micro cold formed parts [6].

Computational Shear Interferometry

Computational shear interferometry is based on measuring the spatial covariance, or mutual intensity,

$$G(x,x+s)=\langle V(x,t)V^{*}(x+s,t)\rangle \qquad (5)$$

of a wave field $V(x,t)$ that has been scattered by or transmitted through an object. In Eq.(5) the

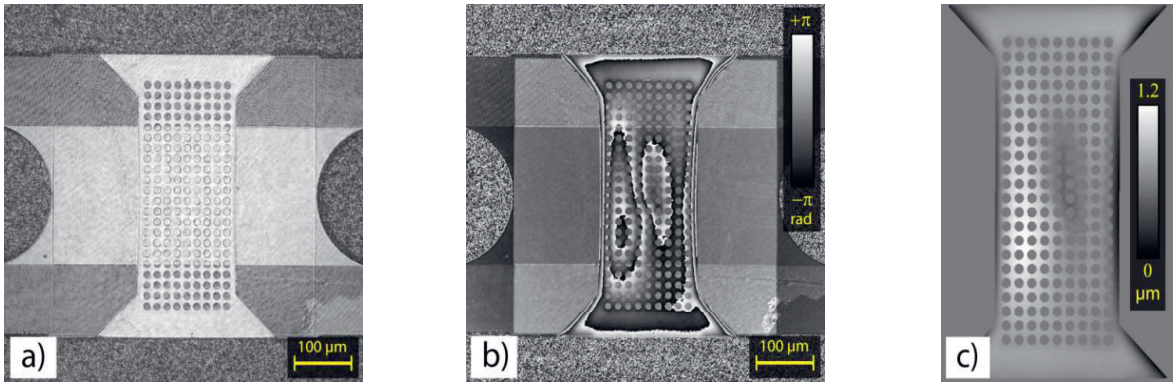

Fig.2.Measuring the shape of a micro-electro-mechanical switch using digital holography: a) The amplitude and b) phase distribution of the light field across the object plane after the numerical propagation process, and c) the shape of the switching bridge as obtained from the phase distribution. All data taken from [5] but evaluated with improved suppression of alias frequencies.

vector s is called the shear and <...> denotes temporal averaging.

Usually a set of mutual intensities $G_n(x,x+s_n)$ with different shears s_n is measured in order to assign a time independent complex amplitude $U(x)$ to it [7].To find $U(x)$, the following objective function has to be minimized

$$L(f)=\sum_n \|G_n(x,x+s_n)-f(x)f^*(x+s_n)\|^2 \quad (6)$$

and thus

$$U(x)=\arg\min_f(L). \quad (7)$$

Minimization of L is not trivial, because it constitutes a non-convex, non-linear problem. It can be accomplished through an iterative gradient descent method with a smart initial guess. The convergence rate can be increased using additional constraints (if applicable) like smoothness for example [7].

If $V(x,t)$ is fully monochromatic, $U(x)$ is the time independent part of $V(x,t)$ and therefore equals the results of phase shifting interferometry or digital holography for example. Hence, CoSI can be employed for a wide range of typical interferometric applications. It combines the robustness, the flexibility and the low coherence requirements of a shear interferometer with the accuracy and the imaging modalities associated with standard interferometry.

Setups for CoSI typically involve a shear interferometer, which is an imaging system that provides two laterally separated images of the same scene. In our experiments we use a 4f-configuration, as seen from Fig.3, with an electronic liquid crystal spatial light modulator (SLM) in the corresponding Fourier domain. The SLM is used to generate a blazed grating which diffracts light only into the first diffraction order. The SLM is a birefringent device. Light which is incident along the slow axis will be diffracted whereas light oriented along the fast axis will be reflected from the silicon back panel of the device. We exploit this behavior by using the first polarizer to adjust the polarization in a 45° angle between the slow and the fast axis. Hence, part of the light is reflected and part of the light is diffracted. This leads to the formation of two images in the back focal plane of the 4f-arrangement. The shift between the images can be controlled by the orientation and the period of the blazed grating. The polarizer in front of the camera sensor is used to let the images interfere. The great advantage of this configuration is that the shift between the images can be electronically changed without the requirement for any mechanically moving parts, which is very precise, reproducible and can be accomplished at video rate.

If the wave field $V(x,t)$ is incident in the object plane, the intensity observed in the image plane of a shear interferometer is given by

$$I(x)=\langle|V(x,t)|^2\rangle+\langle|V(x+s,t)|^2\rangle +2\Re\{G(x,x+s)\} \quad (8)$$

The mutual intensity in the last term on the right hand side can be isolated by means of standard phase shifting techniques [8].

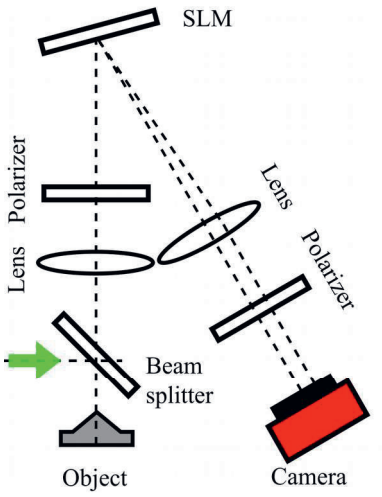

Fig.3.Scheme of a shear interferometer which consists of a 4f-configuration with a reflective liquid crystal SLM in the Fourier plane as the shearing element. The SLM acts as a programmable diffractive element, which generates two identical but mutually shifted images in the camera domain. A plane wave is inserted from the left as indicated by the arrow and the beam splitter is used to provide normally incident object illumination. For further details about the setup please refer to the text.

Please note that even though it provides accuracy in the low nanometer range, CoSI does not require any active or passive mechanical stabilization because of the common path nature of the setup [9].

CoSI has low demands with respect to the coherence of light. However, a mandatory requirement is that the light source is point symmetric [10], so that the mutual intensity function of the object illumination is spatially stationary and real valued. Furthermore, the illumination has to provide spatial coherence at least over the distance given by the shear. These requirements are met, for example, by a fibre coupled light emitting diode (LED). In our experiments we use a Thorlabs M625F2 LED which is coupled into a multi mode fibre with a

core diameter of 400 µm. The LED emits light at 625 nm with a coherence length of l_c=10 µm.

Figure 4 shows some results from the fields of 3D shape measurement and quantitative phase contrast imaging. For both results the objects were investigated in reflection mode and under normally incident light. Figure 4a shows the shape of a micro-electro-mechanical system (MEMS). We used 10 sheared interferograms to arrive at the complex amplitude $U(x)$. To determine the shape, we use again Eq.(4) and apply it to the lateral phase distribution of $U(x)$. In order to avoid ambiguities associated with steps that are larger than half of the wavelength, we apply a multi wavelength contouring approach and evaluate two measurements with different wavelengths in combination [11].

In Fig.4b we used a liquid crystal SLM as object and investigated the phase modulation caused by the liquid crystal cells. To this end, we placed the SLM in the object plane of the shear interferometer to investigate the lateral phase distribution of $U(x)$ before and after changing the pixel values of the SLM. In Fig.4b we see the phase modulation when we let the SLM generate a blazed grating at a 45° angel. The image shows the border region of the SLM, where we can identify the pixelated structure of the liquid crystal cells on the right hand side, which is in accordance with the modulation. On the left side we see the edge of the active area without liquid crystal cells in grey (zero phase modulation). In order to investigate display errors, we subtract the expected blazed grating from the measured phase modulation. The result is shown in Fig.4c, where we can identify dead pixels, non-linear behavior and cross-talk of the device, as indicated by the arrows. The measurement uncertainty for the phase measurement is σ=0.03 rad, which equals 3 nm in optical path. Yet, the system can be operated without any mechanical stabilization.

Conclusions

The above examples demonstrate the strength of CoMet: Because the recorded data does not need to be meaningful to a human observer, we gain additional degrees of freedom in system design. This can be used to tailor the measurement process towards combined benefits, such as precision and speed, as in the case of digital holography or precision and insensitivity to mechanical disturbances as in the case of CoSI.

Having said this, these benefits come at the cost of computational effort, because the computational part often involves highly complex inverse problems. Within this scheme, the recorded intensities are interpreted as an effect that has been caused by an unknown, yet to be recovered, cause. Furthermore, the computational part often makes it more difficult to determine crucial system parameters, such as measurement uncertainty or measurement range.

Fig.4.Two examples of application of CoSI: a) Shape of a MEMS acceleration sensor and b) measured phase modulation of a liquid crystal spatial light modulator (SLM) which displays a 45° blazed diffraction grating. The image shows the edge of the active area of the SLM, where the modulation caused by the liquid crystal cells is seen on the right and the inactive area is recognized on the left side in gray (zero modulation). c) To visualize systematic deviations caused by the SLM, we have subtracted the expected phase modulation from the measurement across the active area of the SLM. On the right side we see non-linear behavior and cross talk of the liquid crystal cells as indicated by the arrows. In the central region we see a vertical stripe of dead pixels which is 4 pixels wide. The corresponding liquid crystal cells are apparently not controlled by the electronics of the SLM.

Acknowledgements

The authors would like to thank the Deutsche Forschungsgemeinschaft (DFG) for funding parts of the work under contracts BE 1924/22-1 (OPAL) and BE 1924/25-1 (Γ-Profilometrie).

References

[1] U. Schnars, C. Falldorf, J. Watson, W. Jüptner, Digital Holography and Wavefront Sensing, Springer (2015)

[2] J. Sheng, E. Malkiel, J. Katz, Digital holographic microscope for measuring three-dimensional particle distributions and motions, Appl. Opt. 45, 3893-3901 (2006); doi: 10.1364/AO.45.003893

[3] S. Seebacher, W. Osten, W. Jüptner, Measuring shape and deformation of small objects using digital holography, in Proc SPIE 3479, 104–115 (1998); doi:10.1117/12.316439

[4] B. Kemper, G. von Bally, Digital holographic microscopy for live cell applications and technical inspection, Appl. Opt. 47, A52-A61 (2008); doi: 10.1364/AO.47.000A52

[5] C. Falldorf, C. von Kopylow, W. Jüptner, Digital holography applied to reflective micro systems, in Technisches Messen 73, 257-265 (2006); doi: 10.1524/teme.2006.73.5.257

[6] A. Simic, C. Falldorf, and R. Bergmann, Internal Inspection of Micro Deep Drawing Parts Using Digital Holography, in Imaging and Applied Optics 2016, paper DW1H.3 (2016); doi: 10.1364/DH.2016.DW1H.3

[7] C. Falldorf, M. Agour, R.B. Bergmann, Digital holography and quantitative phase contrast imaging using computational shear interferometry, Opt. Eng. 54, 024110 (2015); doi: 10.1117/1.OE.54.2.024110

[8] T. Kreis, Handbook of Holographic Interferometry, Wiley-VCH (2005)

[9] R.B. Bergmann, J. Burke, C. Falldorf, Precision optical metrology without lasers, in Proc. SPIE 9524, 952403 (2015); doi: 10.1117/12.2183451

[10] C. Falldorf, Taking the Next Step: The Advantage of Spatial Covariance in Optical Metrology, in Imaging and Applied Optics 2016, paper DW3E.1 (2016); doi: 10.1364/DH.2016.DW3E.1

[11] C. Towers, D. Towers, and J. Jones, Optimum frequency selection in multifrequency interferometry, Opt. Lett. 28, 887-889 (2003); doi: 10.1364/OL.28.000887